[Short title + Author Name - P&H title] 17 (2024) 105865

Contents lists available at ScienceDirect

Arabian Journal of Chemistry

journal homepage: www.ksu.edu.sa

A rearranged abietane diterpenoid from *Clerodendrum mandarinorum* inhibits tumor progression of oral squamous cell carcinoma *in vitro*

Kaidi Xiao [a,b,1], Yuxin Zhu [a,b,1], Yeling Wu [a,b], Bing Li [a,b], Shihao Cai [a], Kaijun Qiu [c], Chaoge Liu [d], Xiaoyu Ai [a], Xiaohe Li [a], Honggang Zhou [a], Ting Xiao [a,*], Chunfeng Xie [a,*], Cheng Yang [a,*]

[a] State Key Laboratory of Medicinal Biology, College of Pharmacy and Tianjin Key Laboratory of Molecular Drug Research, Nankai University, Tianjin 300353, China
[b] Tianjin Key Laboratory of Molecular Drug Research, Tianjin International Joint Academy of Biomedicine, Tianjin 300457, China
[c] College of Basic Sciences, Tianjin Agricultural University, 22 Jinjing Road, Xiqing District, Tianjin 300392, China
[d] Department of Oramaxillofacial - Head and Neck Surgery, Tianjin Stomatological Hospital, School of Medicine, Nankai University, Tianjin 300041, China

ARTICLE INFO

Keywords:
Clerodendrum mandarinorum
Rearranged abietane diterpenoids
Tongue squamous cell carcinoma
Transforming Growth Factor Beta Receptor 2 (TGFβR2)
Epithelial-mesenchymal transition (EMT)

ABSTRACT

Tongue cancer, a prevalent form of oral malignancy, particularly manifests as tongue squamous cell carcinoma (TSCC), which holds the highest incidence among oral squamous cell carcinoma cases, representing 43.4 % of occurrences. Presently, surgical resection stands as the primary treatment for TSCC, with no effective pharmaceutical interventions identified. This study aims to search for the potential anti-tumor properties and molecular mechanisms of a rearranged abietane diterpenoid extracted from *Clerodendrum mandarinorum*. Within this investigation, six known rearranged abietane diterpenoids (**1**–**6**) were isolated and characterized from *C. mandarinorum*. Notably, compound **1** demonstrated the most robust inhibitory effect against CAL-27 cells. Pharmacological assays further substantiated that compound **1** significantly restrained the proliferation, migration, and invasion of CAL-27 cells. Moreover, it was revealed that compound **1** directly interacted with TGFβR2, a pivotal receptor in the downstream signaling pathways of TGF-β/Smad and PI3K/AKT. Transcriptome analysis provided additional confirmation of these observations. Overall, our study highlights the promising potential of compound **1** as a therapeutic agent for the treatment of oral squamous cell carcinoma.

1. Introduction

Head and neck cancer is a broad term encompassing tumors that stems from various regions in the head and neck, including laryngeal, thyroid, oral, nasopharyngeal, and hypopharyngeal areas (Ran and Yang, 2017). It ranks as the sixth most common cancer worldwide and carries a high mortality rate of nearly 50 % (Katzenellenbogen et al., 2018). Squamous cell carcinoma accounts for over 90 % of these cancers. Head and neck squamous cell carcinoma (HNSCC) presents a significant challenge in terms of treatment and patient outcomes. Within the spectrum of Head and Neck Squamous Cell Carcinoma (HNSCC), oral squamous cell carcinoma, notably tongue squamous cell carcinoma, stands out as the most prevalent subtype (Omori et al., 2020). Surgical resection remains a cornerstone in the treatment of tongue squamous cell carcinoma, aiming for complete removal of the tumor and surrounding tissues (De Berardinis et al., 2022). Despite this intervention, the prognosis for patients with this condition remains difficult, highlighting the need for alternative or complementary treatment modalities. In recent years, immunotherapy has emerged as a promising approach in the treatment of various cancers, including HNSCC. PD-1 inhibitors such as nivolumab and pembrolizumab have shown efficacy by enhancing the immune system's ability to target and eliminate tumor cells (Topalian et al., 2020). However, the response rates to these treatments can vary among patients, with a significant proportion showing resistance or limited benefit. Therefore, it is crucial to delve into and identify new therapeutic targets, as well as to devise comprehensive treatment strategies that encompass a variety of therapies.

TGFβR2, a transmembrane protein featuring a protein kinase domain, plays a crucial role in cellular signaling. It forms a complex with TGF-β receptor I (TGFβR1) and binds to TGF-β (Peng et al., 2022;

* Corresponding authors.
E-mail addresses: xiaokaidi2022@163.com (K. Xiao), z15265724088@163.com (Y. Zhu), tingxiao@nankai.edu.cn (T. Xiao), xiechunfeng@nankai.edu.cn (C. Xie), cheng.yang@nankai.edu.cn (C. Yang).
[1] Co authors.

https://doi.org/10.1016/j.arabjc.2024.105865
Received 23 October 2023; Accepted 5 June 2024
Available online 10 June 2024

Massagué, 2008). Upon binding of the ligand, the receptor/ligand complex phosphorylates proteins, leading to its translocation into the cell nucleus where it modulates the transcription of genes linked to various cellular processes like proliferation (Ma et al., 2014), cell cycle arrest (Wang et al., 2012), immune suppression (Zeboudj et al., 2023), and tumor development (Huang et al., 2019). TGFβR2 is involved in TGF-β signaling, which includes downstream pathways such as the classic Smad pathway and non-Smad pathways like PI3K/AKT, NF-κB, and MAPK (Loomans and Andl, 2014). These signaling pathways regulate distinct physiological processes and are closely associated with the initiation and progression of tumors (Peng et al., 2022). The TGF-β signaling pathway, by activating the canonical Smad pathway or non-Smad pathways, induces the expression of transcription factors such as Snail1/2, ZEB1/2, and HMGA2, promoting epithelial-mesenchymal transition. These transcription factors can suppress the expression of epithelial cell adhesion proteins while mediating the expression of mesenchymal proteins. These changes lead to the loss of cell polarity and cell–cell contacts, enabling cells to acquire a migratory and invasive phenotype, facilitating the spread of cancer cells to other tissues (Colak and ten Dijke, 2017).

Clerodendrum mandarinorum Diels, a member of the Verbenaceae family and the *Clerodendrum* genus, is indigenous to Southern China and Northern Vietnam, displaying diverse growth patterns as small trees or shrubs (Editorial Committee of the Flora of China et al., 1982). Historically, the twigs and leaves of *C. mandarinorum* have been utilized in traditional medicine to address conditions like hemiplegia and poliomyelitis (Compilatory Group of Compilation of Chinese Herbal Medicine, 1996). The volatile oil from the leaves of *C. mandarinorum* exhibited the antimicrobial effect (Yang et al., 2018). In addition, the extract from the root barks of *C. mandarinorum* could bind with α1- and α2-adrenoceptors, 5HT-1, 5HT-1A, 5HT-2, opiate, adenosine-l, dopamine 1, GABAA and GABAB receptors (Zhu et al., 1996). Phytochemical studies on this plant species have revealed the presence of rearranged abietane diterpenoids as the main constituents (Fan et al., 1999; Fan et al., 2000). These abietane diterpenoids have been reported to possess significant cytotoxic effects (Wang et al., 2013). However, the potential role of this plant in anti-tumor therapy has not been explored. Hence, we conducted on the extraction and isolation of six known rearranged abietane diterpenoids from this plant, which were characterized as 11-methoxyl-12,14-dihydroxy-13-(2-hydroxypropyl)-3,5,8,11,13-abietapentaen-7-one (**1**), uncinatone (**2**), teuvincenone G (**3**), teuvincenone H (**4**), teuvincenone E (**5**), and villosin B (**6**), respectively. Compound **1** exhibited the promising inhibitory effect on human tongue squamous cell carcinoma CAL-27 cell by binding to TGFβR2 and could become a potential cancer treatment drug.

2. Materials and methods

2.1. General experimental procedures

General experimental procedures for isolation and structure elucidation were included in the Supporting Information.

2.2. Plant material

The twigs and leaves of *Clerodendrum mandarinorum* Diels were collected from Wutai Mountain, Yunnan province, China in October 2020 and identified by one of authors (C. X.). The voucher specimen (No. 202010CM) was deposited at the College of Pharmacy, Nankai University, China.

2.3. Cell lines and cell culture

Human nasopharyngeal carcinoma cells CNE, human oral squamous cell carcinoma cells CAL-27, non-small cell lung cancer cells A549, and pancreatic cancer cells PANC-1 were cultured with RPMI-1640 medium that contained 10 % fetal bovine serum and grown under standard conditions (37 °C, 95 % air atmosphere, 5 % CO_2).

2.4. Cell viability assay

Cells were seeded in 96-well plates at a density of 3000 cells/well, and cultured in a cell culture incubator at 37 °C and 5 % CO_2 for 24 h. Drugs with concentrations of 0 μM, 15 μM, and 30 μM were prepared in their respective culture media and added to the wells of the 96-well plate for a 48-hour incubation period. MTT (Thiazolyl Blue) solution (5 mg/ml) was co-incubated with the cells at 37 °C and 5 % CO_2 for 4 h to assess cells viability. The blue-purple crystals formed in the 96-well plate were completely dissolved using Dimethyl sulfoxide (DMSO), and the absorbance (OD value) was measured at a wavelength of 570 nm by a microplate reader. The obtained data was analyzed by GraphPad Prism 9.0 (Stockert et al., 2018).

2.5. EDU (5-ethynyl-2-deoxyuridine) cell proliferation assay

The experiment involved treating CAL-27 cells with various concentrations of compound **1** for 24 h. After the treatment period, the cells were incubated with EDU working solution for 2 h. This solution specifically labels newly proliferated cell DNA molecules. Following the incubation with the EDU working solution, the cells were fixed and permeabilized to prepare them for further analysis. A click reaction solution was added to the cells at room temperature, and then the cells were incubated in darkness for a duration of 30 min. This click reaction solution reacts with the EDU-labeled DNA molecules, allowing for their easy detection and visualization. Finally, the labeling status of the cells was determined using a specialized instrument called a confocal microscope (Xiao et al., 2023).

2.6. Wound healing assay

To initiate the experiment, prepare a 24 well plate with a specific cell density of 3×10^5 cells per well. Gently glide a sterilized pipette tip across the well surface, ensuring consistent size and depth of the scratch gaps created. Once the scratch gaps are formed, cautiously add RPMI-1640 medium to each well, ensuring that the medium contains different concentrations of the drugs under investigation. Capture images of the scratch gaps at 0, 12, 24, and 36 h post-treatment. Software tools such as Image J and GraphPad Prism9.0 were employed for analysis and data processing (Lin et al., 2022).

2.7. Transwell assay

Mix matrigel and RPMI-1640 medium in a ratio of 1:3. Then add this mixture to the transwell chamber and let it to stand for 30 min at a temperature of 37 °C. Before seeding the cells, it is important to hydrate the basal membrane. This can be achieved by adding a culture medium containing 0.1 % fetal bovine serum to the transwell chamber and incubating it for 30 min. Next, collect the desired cells and resuspend them in a culture medium containing 0.1 % fetal bovine serum. 2×10^5 cells were added to each transwell chamber. To induce cell invasion, add a complete culture medium to the lower layer of the transwell chamber. Place the transwell chamber in a cell culture incubator set to a temperature of 37 °C and a CO_2 concentration of 5 %. Allow the cells to invade for 24 h. Remove any remaining cells from the upper side of the transwell chamber by gently wiping it with a cotton swab. After removing the residual cells, fix the cells that have invaded the lower side of the transwell chamber by adding 4 % cell fixative to the chamber and incubating it for 30 min. Finally, stain the cells with crystal violet dye. After staining, the cells can be observed and captured under a microscope for further analysis (Xiao et al., 2023).

2.8. Colony formation experiment

The cells were digested with pancreatic enzyme and collected by centrifugation. Subsequently, the cells were seeded into 6-well plates at a density of 300 cells per well. After 24 h of incubation, different concentrations of compound **1** were added to the wells. The plates were then placed in a cell culture incubator set at 37 °C and 5 %CO_2 for a period of 7 days. After incubation, the cells were fixed with 4 % cell fixative solution for 30 min. Following fixation, the cells were stained with a crystal violet solution. To quantify the number of cell clones, statistical analysis was performed using the Image J (Xiao et al., 2023).

2.9. Cellular thermal shift assay

The cells were initially treated with either PBS or compound **1** (30 μM) for 24 h. After this treatment, the cells were digested using pancreatic enzymes and collected by centrifugation. The cells suspended in PBS underwent another round of centrifugation. To prepare the samples for further analysis, the cells were re-suspended in RIPA lysate, which contained equal amounts of either PBS or compound **1**. The cell suspension was divided into separate EP tubes, with each tube containing 80 μL of the cell suspension. Next, the cells in each tube were exposed to different temperatures ranging from 45 °C to 75 °C for a duration of 5 min each. Following the heating process, the cells were rapidly frozen in liquid nitrogen. This freezing and thawing process was repeated three times. After the freezing-thawing cycles, the cell lysate obtained from the samples was centrifuged at a rotating speed of 20,000×g for 20 min at a temperature of 4 °C. The supernatant was collected for further analysis using western blot (Jafari et al., 2014).

2.10. Western blotting

CAL-27 cells were treated with different concentrations of compound **1** (0 μM, 15 μM and 30 μM) for 24 h. After the treatment, RIPA lysate was added to the cells to collect the total protein. The protein concentration was measured using the BCA reagent. To further analyze the protein samples, the same samples were separated using a 10 % gel and transferred to a PVDF membrane. The PVDF membrane was sealed with 5 % skim milk for 1 h to ensure proper binding. Subsequently, the primary antibody was incubated with the membrane overnight at 4 °C. The second antibody was added to the membrane and incubated at room temperature for 2 h. The protein expression bands corresponding to the target proteins were detected using a chemiluminescence detector. The resulting images were quantitatively analyzed by Image J (Lin et al., 2022).

2.11. qRT-PCR

In this experiment, total RNA was extracted using the Trizol reagent. After extraction, the concentration of the RNA was measured using a microspectrophotometer, which enables precise quantification of nucleic acids by measuring their absorbance. The Fastking gDNA Dispelling RT Super Mix was used to perform reverse transcription synthesis of cDNA. This kit contains all the necessary components, including enzymes and primers, to effective conversion of RNA into complementary DNA (cDNA). For the subsequent quantitative polymerase chain reaction (qPCR), we used the Unicon qPCR SYBR Green Master Mix. This mix contains a fluorescent dye, SYBR Green, which binds to the newly synthesized DNA during the amplification process. The abundance of the target gene in the sample was measured by monitoring the increase in fluorescence (Xiao et al., 2023).

2.12. Immunofluorescence

CAL-27 cells were cultured on a cell creep in a 24-well plate for 24 h. Afterward, they were treated with various concentrations of compound **1** for an additional 24 h. Following this, the cells were fixed using a 4 % cell fixative solution for 30 min. To ensure effective permeability of the cell membrane, 0.2 % Triton X-100 was used. Additionally, to block any non-specific binding of proteins, 5 % BSA was applied. The primary antibody was then incubated overnight at a temperature of 4 °C, and the secondary antibody was incubated at room temperature for 2 h. The cell nuclei were stained using DAPI, and finally, the coverslip was sealed. The staining was subsequently observed using a confocal microscope (Xiao et al., 2023).

2.13. Statistical analysis

All experiments were performed in triplicates at least, all statistical analyses were performed using GraphPad Prism 8.0. The data are expressed as mean ± standard deviation (SD). The *t*-test was performed to compare the significant difference of the means between the two groups. All results were quantified using ImageJ software (NIH, Bethesda, MD, USA). *$p < 0.05$, **$p < 0.01$, ***$p < 0.001$, ****$p < 0.0001$, $^{\#}p < 0.05$, $^{\#\#}p < 0.01$, $^{\#\#\#}p < 0.001$, and $^{\#\#\#\#}p < 0.0001$ were considered statistically significant.

3. Results

3.1. Structural identification of compounds 1–6

The EtOAc-soluble layer from the methanol extract of the twigs and leaves of *C. mandarinorum* afforded six known rearranged abietane diterpenoids (Fig. 1), which were identified as 11-methoxyl-12,14-dihydroxy-13-(2-hydroxypropyl)-3,5,8,11,13-abietapentaen-7-one (**1**) (Xu et al., 2010), uncinatone (7,11-dihydroxy-3,4,9,11b-tetramethyl-1,2,8,9,11b-pentahydrophenanthro[3,2-*b*]furan-6(2*H*)-one, **2**) (Tian et al., 1993), teuvincenone G [(16*S*)-12,16-epoxy-11,14-dihydroxy-17(15 → 16)-*abeo*-abieta-8,11,13-triene-3,7-dione, **3**] (Cuadrado et al., 1992), teuvincenone H (12,16-epoxy-6,11,14-trihydroxy-17(15 → 16)-*abeo*-abieta-5,8,11,13,15-pentaene-3,7-dione, **4**) (Pinheiro Barros et al., 2003), teuvincenone E [(16*S*)-12,16-epoxy-11,14-dihydroxy-17(15 → 16),18(4 → 3)-*diabeo*-abieta-3,5,8,11,13-pentaene-2,7-dione, **5**] (Rodríguez, 2002), and villosin B [(5S,10S,16R)-12,16-epoxy-11,14,17-trihydroxy17(15 → 16)-*abeo*-abieta-8,11,13-triene-7-one, **6**] (Li et al., 2014) by comparison of their spectroscopic data with those previously reported in the literature (Supporting Information). For compound **1**, the ^{1}H NMR spectrum exhibited the presence of one methoxy group at δ_H 3.80 (s, 3H), four methyl groups at δ_H 1.15 (d, $J = 6.2$ Hz, 3H), 1.52 (s, 3H), 1.91 (s, 3H), 1.94 (s, 3H), one olefinic methine at δ_H 6.22 (s, 1H), and one oxygenated methine at δ_H 4.13 (s, 1H). The ^{13}C NMR data revealed the presence of 21 carbon resonances, including one methoxy group at δ_C 61.3, one ketone at δ_C 192.2, one oxymethine at δ_C 68.1 and ten olefinic carbon resonances at δ_C 168.8, 156.4, 154.9, 143.1, 141.6, 136.1, 126.3, 119.6, 119.0, and 112.1. The absolute configurations at C-10 and C-16 were demonstrated as 10*S* and 16*R* according to ECD curve (Fig. S3, Murata et al., 2016; Fan et al., 2000) and comparison of the key ^{13}C NMR data with the known analogue szemaoenoid C, whose absolute configuration was established by X-ray diffraction analysis (Table S1, Pu et al., 2018). The ^{13}C NMR data of compound **3** was also provided for the first time in the Table S2 based on the 2D-NMR spectra.

3.2. Compound 1 inhibits the proliferation, migration and invasion of oral squamous cell carcinoma in vitro

The effectiveness of all compounds except compound **3** and compound **5** (due to limited amount available) in inhibiting the growth of four types of human tumor cells, including CNE, CAL-27, A549 and PANC-1, was tested *in vitro*. The results showed that compound **1** exhibited the highest level of inhibition on CAL-27. At a concentration of 65.63 μM, half of the inhibitory effect on CAL-27 was achieved (Fig. 2A and B). Moreover, to further investigate the impact of compound **1** on

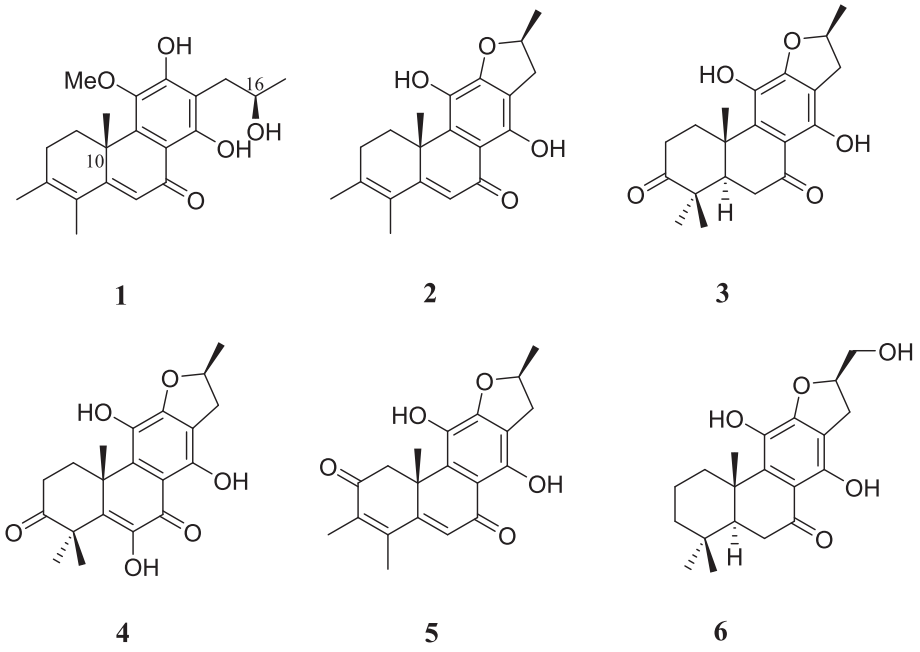

Fig. 1. Chemical structures of compounds **1**–**6**.

CAL-27 proliferation, MTT assay and EdU cell proliferation assay were conducted, both of which demonstrated a dose-dependent inhibition patter (Fig. 2C and D). These assays provided evidence that compound **1** suppressed the proliferation of CAL-27. Additionally, the migration behavior of CAL-27 was examined using a wound healing assay. The results indicated that compound **1** significantly hindered the migration of CAL-27, with the level of inhibition increasing as the concentration of compound **1** increased (Fig. 2E). Furthermore, the result of transwell assay confirmed that compound **1** also effectively inhibited the invasive behavior of CAL-27. Similar to the pattern observed for proliferation inhibition, this inhibitory effect was also found to be dose-dependent (Fig. 2F). Lastly, a colony formation experiment was conducted to assess the impact of compound **1** on the colony formation ability of CAL-27. The results revealed that compound **1** significantly suppressed the ability of CAL-27 to form colonies (Fig. 2G). Overall, these findings demonstrate that compound **1** derived from *C. mandarinorum* possesses potent antitumor properties, particularly in inhibiting the growth, proliferation, migration, invasion and colony formation abilities of CAL-27, highlighting its potential as a promising therapeutic candidate for tongue squamous cell carcinoma treatment.

*3.3. Compound **1** inhibits the activation of the TGF-β/Smad and PI3K/AKT pathways, as well as epithelial-mesenchymal transition (EMT), through specific binding to TGFβR2*

To further investigate the mechanism by which compound **1** inhibited tumor cell proliferation and metastasis, the PharmMapper database was used to predict its potential binding targets. It was discovered that compound **1** had a strong likelihood of binding to TGFβR2. This finding is particularly significant considering previous studies linking TGFβR2 to tumor development and metastasis (Xie et al., 2022). To authenticate the interaction between compound **1** and TGFβR2, molecular docking was employed. The results revealed that compound **1** bound to three specific amino acid residues (LYS277, ALA326, and ASP397) within the TGFβR2 structure (PDB ID 5E8V). Compound **1** occupied the protein kinase domain of TGFβR2 by interacting with the three amino acid residues, thereby inhibiting the formation of heterodimers and the activation of downstream signaling pathways. Furthermore, computer simulations were conducted to calculate the binding energy between compound **1** and TGFβR2, confirming their strong affinity (Fig. 3A). To further verify the binding between compound **1** and TGFβR2, a cellular thermal shift assay was performed. By subjecting the protein to increasing temperatures, a pronounced decrease in the protein degradation rate of TGFβR2 was observed in the presence of compound **1** compared to the control group treated with PBS (Fig. 3B). This provides compelling evidence for the binding interaction between compound **1** and TGFβR2 and supports the notion that compound **1** may play a role in inhibiting tumor cell proliferation and metastasis through its interaction with TGFβR2.

TGFβR2 plays a crucial role in the TGF-β signaling pathway, which is involved in various cellular processes. In addition to the classical TGF-β/Smad pathway, TGFβR2 also activates non-classical pathways, including Wnt/β-catenin, PI3K/AKT, and NF-κB (Loomans and Andl, 2014). Previous studies have established the significance of the TGF-β/Smad pathway in tumor metastasis and progression, as well as the role of the PI3K/AKT pathway in non-classical signaling. To investigate the effects of compound **1** on these pathways, western blot analysis was performed to measure the phosphorylation levels of key proteins involved. The results demonstrated that compound **1** significantly decreased the phosphorylation levels of Smad2, Smad3, PI3K, and AKT (Fig. 3C and D). This indicated that compound **1** suppressed the activation of both the classical and non-classical TGF-β signaling pathways. Furthermore, compound **1** also influenced the expression of epithelial-mesenchymal transition (EMT) markers, which were regulated by the TGF-β signaling pathway. Immunoblotting analysis showed a reduction in the expression levels of Twist1, vimentin, and N-cadherin, while the expression of E-cadherin increased (Fig. 3E). Similarly, mRNA expression levels of vimentin and N-cadherin decreased, while the mRNA levels of E-cadherin increased (Fig. 3F). These findings suggest that compound **1** inhibits the occurrence of EMT, a crucial process for tumor metastasis. To further confirm these results, immunofluorescence staining was performed, which supported previous findings (Fig. 3G). Taken together, these results provide strong evidence that compound **1** effectively hinders the progression of EMT, thereby potentially suppressing tumor metastasis.

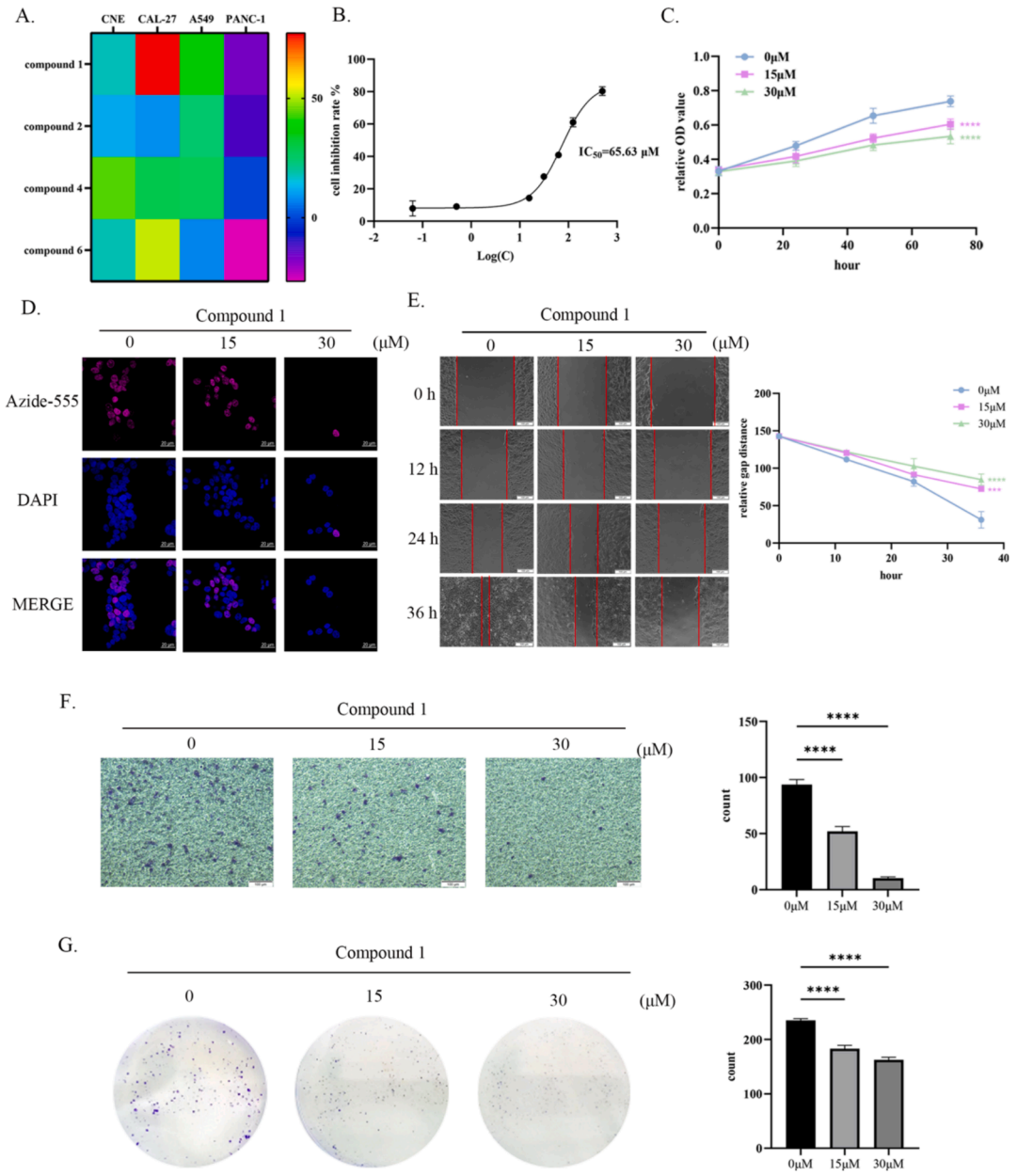

Fig. 2. Compound 1 inhibited the proliferation, migration and invasion of CAL-27 *in vitro*. (A) Through MTT assay, the inhibitory rates of compounds **1**, **2**, **4**, and **6** on four types of tumor cells were detected. (B) The half inhibitory concentration of the compound **1** on CAL-27 cells was tested by MTT assay. (C) MTT assay was used to determine the proliferation inhibition rate of compound **1** on Cal27 cells at concentrations of 0 μM, 15 μM, and 30 μM. (D) Expose CAL-27 to compound **1** at concentrations of 0 μM, 15 μM, and 30 μM for 24 h, then tested EDU fluorescence intensity. (E) Compound **1** inhibited wound healing of CAL-27 in a concentration-dependent manner. (F) Compound **1** inhibited the invasive ability of CAL-27 in a concentration-dependent manner. (G) Compound **1** inhibited the clonogenicity of CAL-27 in a concentration-dependent manner. ****$p < 0.0001$.

*3.4. Transcriptome sequencing confirmed the inhibitory effect of compound **1** on TGF-β/smad and PI3K/AKT pathways*

Furthermore, to gain a deeper understanding of the impact of compound **1** on CAL-27, RNA sequencing was utilized to analyze two distinct groups of cells: one treated with compound **1** and the other without treatment. The results depicted on the heat maps clearly showed notable differences in gene expression between these two groups (Fig. 4A). Additionally, the volcano plot provided intriguing insights, revealing that a total of 1556 genes were up-regulated, while 2438 genes were down-regulated in the cells treated with compound **1** compared to the untreated cells (Fig. 4B). To explore the biological significance of these differentially expressed genes, GO and KEGG cluster analysis was conducted. This analysis revealed that these genes were primarily associated with crucial processes such as protein biosynthesis and degradation, as well as significant diseases such as type II diabetes and human papillomavirus infection. Moreover, the enriched pathways obtained from the analysis included the TGF-β signaling pathway and the PI3K/AKT signaling pathway (Fig. 4C and D). These results are consistent with the *in vitro* research results mentioned above.

4. Discussion

In the realm of modern drug research and innovation, natural products continue to hold immense significance (Zhang et al., 2020). Natural products, derived from plants, animals, fungi, and microorganisms, have served as a vital source of bioactive compounds that have been developed into numerous pharmaceuticals. These compounds

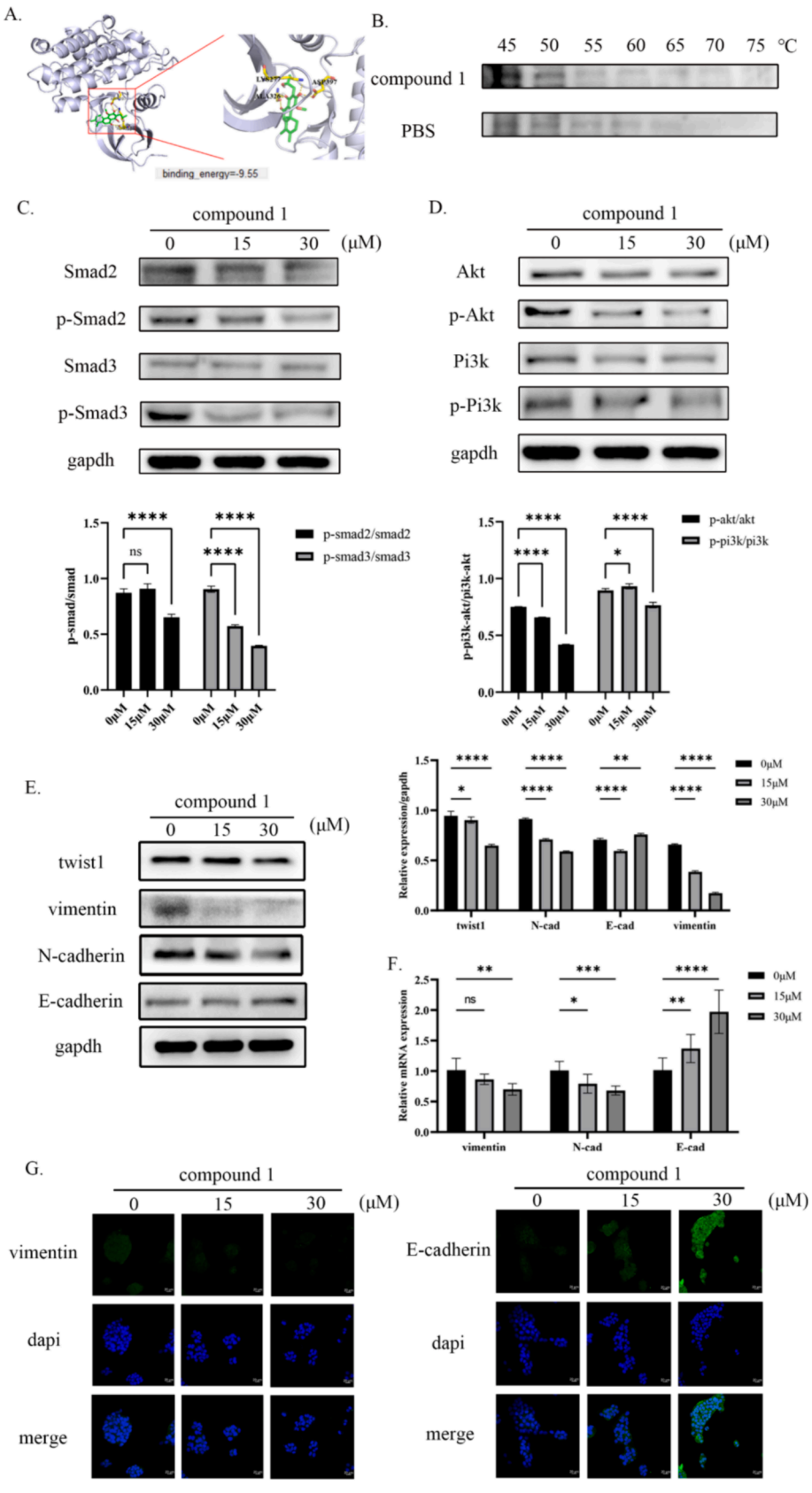

(caption on next page)

Fig. 3. Compound 1 targets TGFβR2 *in vitro*, inhibiting the PI3K/AKT and TGF-β/Smad pathways as well as the EMT process. (A) Virtual molecule docking of compound **1** with TGFβR2 and binding energy between the two. (B) The binding ability of compound **1** to TGFβR2 was verified by cell heat transfer assay (C) The inhibition of TGF-β/Smad pathway activation by compound **1** was confirmed by Western blot (D) The inhibition of PI3K/AKT pathway activation by compound **1** was confirmed by Western blot (E) The protein expression levels of EMT process markers were detected by western blot. (F) The mRNA expression levels of EMT process markers were detected by qRT-PCR. (G) The protein expression levels of EMT process markers were detected by immunofluorescence. $^{ns}p > 0.05$, $^{*}p < 0.05$, $^{**}p < 0.01$, $^{***}p < 0.001$, $^{****}p < 0.0001$.

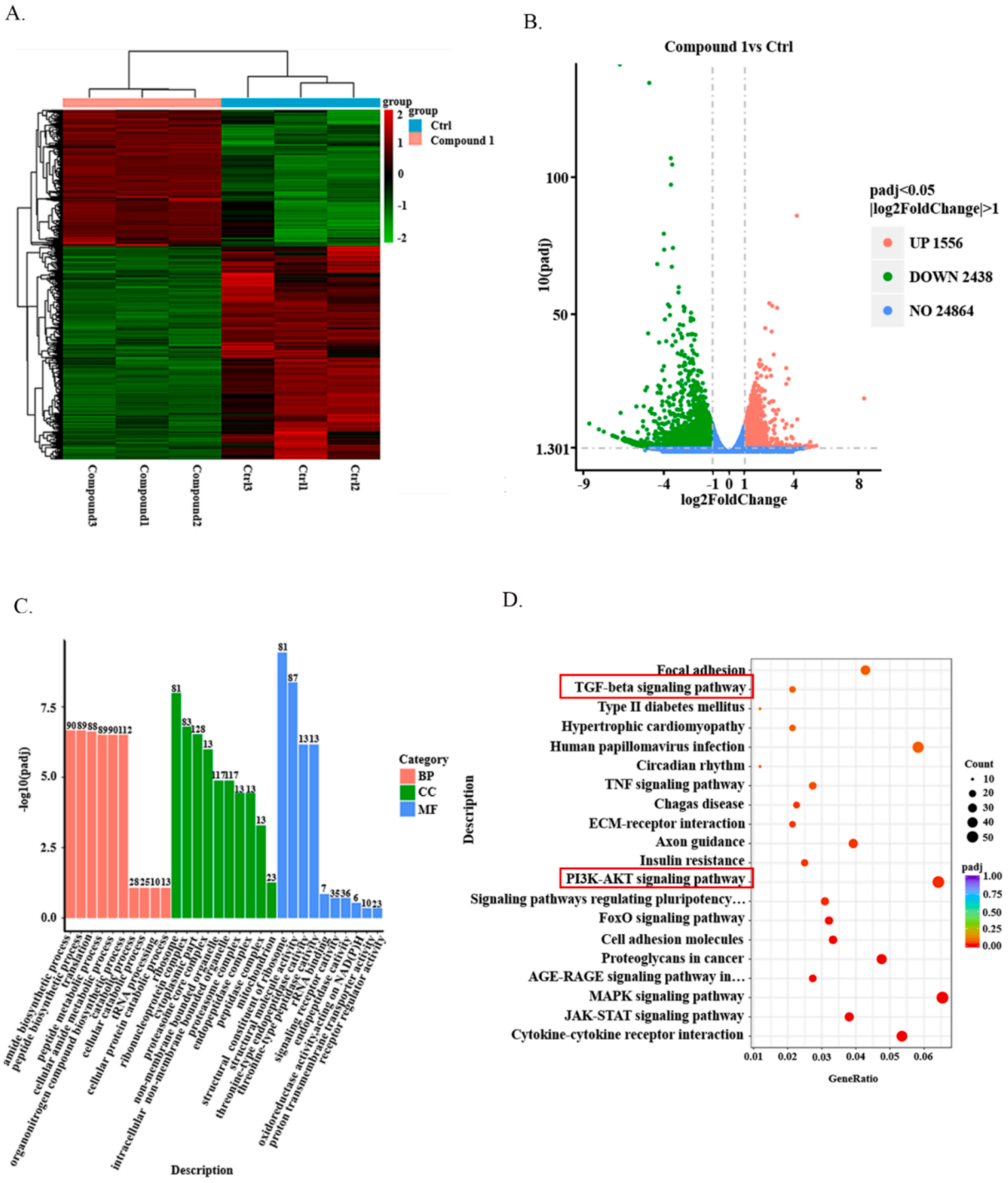

Fig. 4. Transcriptome analysis. (A)Heat maps show the differential genes of CAL-27 cells treated with compound **1** for 24 h versus untreated cells. (B) The volcano map showed the number of up-regulated and down-regulated genes in CAL-27 cells treated with compound **1** for 24 h and in untreated CAL-27 cells. (C) GO analyses the biological processes and related diseases in which differential genes are enriched. (D) KEGG analyzed the related pathways of differential gene enrichment.

often possess diverse chemical structures and biological activities, making them valuable for drug discovery and development (Harvey et al., 2010). Indeed, natural products have played a significant role in the development of anti-tumor medications, with paclitaxel serving as a remarkable example. Paclitaxel, a compound classified within the diterpenoid family, is sourced from the bark of *Taxus brevifolia*, commonly known as the Pacific yew tree. This natural product has garnered substantial recognition and acceptance in clinical practice owing to its efficacy in treating a range of cancer types (Kumar et al., 2016). Camptothecin is another significant natural compound derived from *Camptotheca acuminata*. This compound has garnered attention for its potent anticancer properties and has been utilized in the clinical treatment of various cancers, including acute leukemia, malignant lymphoma, and germ cell tumors (Škubník et al., 2021). The discovery and development of camptothecin and paclitaxel exemplify the potential of natural products in oncology research and drug development.

As a perennial herb, *C. mandarinorum* has been used in China to treat sequelae of hemiplegia and poliomyelitis (Compilatory Group of Compilation of Chinese Herbal Medicine, 1996). However, the anti-tumor activity of *C. mandarinorum* have not yet been discovered sufficiently. Therefore, we extracted and isolated six compounds from the plant *C. mandarinorum* and tested their anti-tumor activity. To evaluate the potential anti-tumor effects of these compounds, a series of experiments were conducted on four different tumor cell lines. The results indicated that compound **1** exhibited the highest level of toxicity against CAL-27 specifically. Additional phenotype experiments were performed to investigate its effects, revealing that compound **1** effectively hindered the proliferation and metastasis of CAL-27 cells. To understand the underlying mechanism of the action of compound **1** on CAL-27, a comprehensive approach was employed, including target prediction algorithms, molecular docking simulations, and cellular thermal shift assays and TGFβR2 was identified as the specific binding target of compound **1** in CAL-27. TGFβR2 is a transmembrane protein that includes a protein kinase domain. It interacts with TGF-β receptor I to form a complex and binds to TGF-β (Liu et al., 2017). Upon ligand binding, this receptor/ligand complex phosphorylates proteins, translocate into the cell nucleus, and orchestrates the transcription of genes linked to vital cellular processes (Peng et al., 2022; Massagué, 2008). Previous studies have linked TGFβR2 to tumor cell proliferation (Liu et al., 2018; Sun, 2009). Specifically, transfecting adenoma cells with functionally deficient TGFβR2 resulted in the cessation of their unlimited proliferation. Subsequent investigations revealed that this transfection of functionally deficient TGFβR2 induced a transition of the adenoma cells, originally displaying mesenchymal characteristics, into cells with epithelial traits, thereby inhibiting their proliferation (Sun, 2009). Our findings align with prior experimental data suggesting that compound **1** may exert its anti-tumor properties by specifically binding to TGFβR2, causing the loss of its functionality and ultimately impeding the proliferation of CAL-27 cells.

The epithelial-mesenchymal transition (EMT) is a critical biological process implicated in tumor metastasis and invasion (Pastushenko and Blanpain, 2019). During tumor metastasis, EMT marker proteins like N-cadherin and vimentin are typically upregulated, while the expression of E-cadherin is downregulated (Nieto et al., 2016; Huang et al., 2022). These changes in protein expression patterns align with previous findings and underscore the role of EMT in driving tumor progression. Studies have indicated that inhibiting the activity of TGFβR2 can weaken the process of epithelial-mesenchymal transition (Bai et al., 2022; Sun et al., 2022; Du et al., 2021). In our research, the discovery that compound **1** can modulate the expression of specific marker proteins associated with EMT, either increasing or decreasing their levels, is consistent with the previous findings. This suggests that compound **1** may exert its anti-tumor metastasis function by targeting TGFβR2 to inhibit EMT.

Numerous studies have extensively delved into the signaling pathways downstream of TGFβR2 in head and neck tumors, prominently focusing on the PI3K/AKT and TGF-β/Smad pathways (Zhang et al., 2020; Zheng et al., 2018; Kim et al., 2019; Wang et al., 2020a,b; Song et al., 2021; Hu et al., 2023). Notably, compound **1** exhibited a notable capacity to inhibit the phosphorylation of key proteins within these pathways. This is consistent with previous research findings. To validate these observations, transcriptome analysis was conducted, unveiling the significant impact of compound **1** on the PI3K/AKT and TGF-β-associated signaling pathways. This comprehensive analysis furnishes additional evidence supporting the ability of compound **1** to modulate these specific pathways effectively.

Although compound **1** has shown promising results in inhibiting tumor growth and migration *in vitro*, its potential *in vivo* anti-tumor effects remain unknown. Therefore, further research is crucial to investigate whether this compound possesses sufficient drug ability for use in medical treatments.

5. Conclusion

Compound **1**, one rearranged abietane diterpenoid isolated from *C. mandarinorum*, exhibits the best anti-tumor activity and inhibits cell migration, invasion, and proliferation of oral squamous cell carcinoma by targeting TGFβR2. It also blocks the activation of downstream signaling such as TGF-β/Smad, PI3K/AKT pathway and EMT by interacting with TGFβR2. Compound **1** deserves further investigation as an anticancer candidate against oral squamous cell carcinoma.

6. Author contributios

Cheng Yang, Chunfeng Xie and Ting Xiao conceived and designed the experiments. Kaidi Xiao and Yuxin Zhu performed all the experiments. Yeling Wu, Bing Li, Shihao Cai, Kaijun Qiu, Chaoge Liu, Xiaoyu Ai, Xiaohe Li and Honggang Zhou analyzed the data. Kaidi Xiao and Ting Xiao wrote the manuscript. All authors read and approved the final manuscript. All data were generated in-house, and no paper mill was used. All authors agree to be accountable for all aspects of work ensuring integrity and accuracy.

7. Informed consent statement

Informed consent was obtained from all subjects involved in the study.

CRediT authorship contribution statement

Kaidi Xiao: Data curation, Methodology, Writing – original draft. **Yuxin Zhu:** Data curation, Methodology. **Yeling Wu:** Formal analysis, Methodology. **Bing Li:** Formal analysis, Methodology. **Shihao Cai:** Investigation. **Kaijun Qiu:** Investigation. **Chaoge Liu:** Investigation, Resources. **Xiaoyu Ai:** Validation, Funding acquisition. **Xiaohe Li:** Visualization. **Honggang Zhou:** Supervision. **Tingxiao:** . **Chunfeng Xie:** Supervision, Writing – original draft, Writing – review & editing. **Cheng Yang:** Supervision.

Declaration of competing interest

The authors declare that they have no known competing financial interests or personal relationships that could have appeared to influence the work reported in this paper.

Acknowledgments

This study was supported by the National Natural Science Foundation of China, China [Grant 82203779]; the Natural Science Foundation of Tianjin, China [Grant 22JCQNJC01610] and the Foundation of Organ Fibrosis Drug Ability Joint Research Centre of Nankai and Guokaixingcheng, China [Grant 735-F1040051]. This study also supported by

the 111 Project B20016, China.

Appendix A. Supplementary data

Supplementary data to this article can be found online at https://doi.org/10.1016/j.arabjc.2024.105865.

References

Bai, F., Wang, C., Liu, X., Hollern, D., Liu, S., Fan, C., Liu, C., Ren, S., Herschkowitz, J.I., Zhu, W.-G., Pei, X.-H., 2022. Loss of function of BRCA1 promotes EMT in mammary tumors through activation of TGFβR2 signaling pathway. Cell Death Dis. 13 https://doi.org/10.1038/s41419-022-04646-7.

Colak, S., ten Dijke, P., 2017. Targeting TGF-β Signaling in Cancer. Trends Cancer 3, 56–71. https://doi.org/10.1016/j.trecan.2016.11.008.

Compilatory Group of Compilation of Chinese Herbal Medicine, 1996. Compilation of Chinese herbal medicine People's Health Press, Beijing, 572-573.

Cuadrado, M.J.S., Bruno, M., De La Torre, M.C., Piozzi, F., Savona, G., Rodríguez, B., 1992. Rearranged abietane diterpenoids from the root of two *Teucrium* species. Phytochemistry 31, 1697–1701. https://doi.org/10.1016/0031-9422(92)83131-h.

De Berardinis, R., Tagliabue, M., Belloni, P., Gandini, S., Scaglione, D., Maffini, F., Margherini, S., Riccio, S., Giugliano, G., Bruschini, R., Chu, F., Ansarin, M., 2022. Tongue cancer treatment and oncological outcomes: The role of glossectomy classification. Surg. Oncol. 42 https://doi.org/10.1016/j.suronc.2022.101751.

Du, H., Gu, J., Peng, Q., Wang, X., Liu, L., Shu, X., He, Q., Tan, Y., Hasnain, M.S., 2021. Berberine suppresses EMT in liver and gastric carcinoma cells through combination with TGFβR regulating TGF-β/Smad pathway. Oxid. Med. Cell. Longev. 2021, 1–21. https://doi.org/10.1155/2021/2337818.

Editorial Committee of the Flora of China, Chinese Academy of Sciences, 1982. Flora of China, 65(1). Science Press, Beijing, p. 185.

Fan, T., Min, Z., Song, G., Iinuma, M., Tanaka, T., 1999. Abietane diterpenoids from *Clerodendrum mandarinorum*. Phytochemistry 51, 1005–1008. https://doi.org/10.1016/s0031-9422(99)00147-8.

Fan, T.-P., Min, Z.-D., Iinuma, M., Tanaka, T., 2000. Rearranged abietane diterpenoids from *Clerodendrum mandarinorum*. J. Asian Nat. Products Res. 2, 237–243. https://doi.org/10.1080/10286020008039917.

Harvey, A.L., Clark, R.L., Mackay, S.P., Johnston, B.F., 2010. Current strategies for drug discovery through natural products. Expert Opin. Drug Discov. 5, 559–568. https://doi.org/10.1517/17460441.2010.488263.

Hu, J., Li, G., Liu, Z., Ma, H., Yuan, W., Lu, Z., Zhang, D., Ling, H., Zhang, F., Liu, Y., Liu, C., Qiu, Y., 2023. Bicarbonate transporter SLC4A7 promotes EMT and metastasis of HNSCC by activating the PI3K/AKT/mTOR signaling pathway. Mol. Carcinog. 62, 628–640. https://doi.org/10.1002/mc.23511.

Huang, Y., Hong, W., Wei, X., 2022. The molecular mechanisms and therapeutic strategies of EMT in tumor progression and metastasis. J. Hematol. Oncol. 15 https://doi.org/10.1186/s13045-022-01347-8.

Huang, H., Zhang, Y., Gallegos, V., Sorrelle, N., Zaid, M.M., Toombs, J., Du, W., Wright, S., Hagopian, M., Wang, Z., Hosein, A.N., Sathe, A.A., Xing, C., Koay, E.J., Driscoll, K.E., Brekken, R.A., 2019. Targeting TGFβR2-mutant tumors exposes vulnerabilities to stromal TGFβ blockade in pancreatic cancer. EMBO Mol. Med. 11. https://doi.org/10.15252/emmm.201910515.

Jafari, R., Almqvist, H., Axelsson, H., Ignatushchenko, M., Lundbäck, T., Nordlund, P., Molina, D.M., 2014. The cellular thermal shift assay for evaluating drug target interactions in cells. Nat. Protoc. 9, 2100–2122. https://doi.org/10.1038/nprot.2014.138.

Katzenellenbogen, J.A., Mayne, C.G., Katzenellenbogen, B.S., Greene, G.L., Chandarlapaty, S., 2018. Structural underpinnings of oestrogen receptor mutations in endocrine therapy resistance. Nat. Rev. Cancer 18, 377–388. https://doi.org/10.1038/s41568-018-0001-z.

Kim, N., Ryu, H., Kim, S., Joo, M., Jeon, H.J., Lee, M.-W., Song, I.-C., Kim, M.-N., Kim, J.-M., Lee, H.J., 2019. CXCR7 promotes migration and invasion in head and neck squamous cell carcinoma by upregulating TGF-β1/Smad2/3 signaling. Sci. Rep. 9 https://doi.org/10.1038/s41598-019-54705-x.

Kumar, P., Raza, K., Kaushik, L., Malik, R., Arora, S., Katare, O., 2016. Role of colloidal drug delivery carriers in taxane-mediated chemotherapy: a review. Curr. Pharm. Des. 22, 5127–5143. https://doi.org/10.2174/1381612822666160524144926.

Li, L., Wu, L., Wang, M., Sun, J., Liang, J., 2014. Abietane diterpenoids from *Clerodendrum trichotomum* and correction of NMR data of Villosin C and B. Nat. Prod. Commun. 9, 907–910.

Lin, R., Sun, R., Xiao, T., Pei, S., Zhang, Q., Cheng, Y., Guo, X., Yang, Z., Gu, X., Zhang, F., Xie, C., Yang, C., 2022. Phenylpropenol ester and sesquiterpenoids with antimetastatic activities from the whole plants of *Chloranthus japonicus*. Arab. J. Chem. 15 https://doi.org/10.1016/j.arabjc.2022.104100.

Liu, S., Chen, S., Zeng, J., 2017. TGF-β signaling: a complex role in tumorigenesis (Review). Mol. Med. Rep. https://doi.org/10.3892/mmr.2017.7970.

Liu, J.-J., Zhang, X., Wu, X.-H., 2018. miR-93 Promotes the growth and invasion of prostate cancer by upregulating its target genes TGFBR2, ITGB8, and LATS2. Mol. Ther. Oncolytics 11, 14–19. https://doi.org/10.1016/j.omto.2018.08.001.

Loomans, H.A., Andl, C.D., 2014. Intertwining of activin A and TGFbeta signaling: dual roles in cancer progression and cancer cell invasion. Cancers (basel). 7, 70–91. https://doi.org/10.3390/cancers7010070.

Ma, Z.-L., Hou, P.-P., Li, Y.-L., Wang, D.-T., Yuan, T.-W., Wei, J.-L., Zhao, B.-T., Lou, J.-T., Zhao, X.-T., Jin, Y., Jin, Y.-X., 2014. MicroRNA-34a inhibits the proliferation and promotes the apoptosis of non-small cell lung cancer H1299 cell line by targeting TGFβR2. Tumor Biol. 36, 2481–2490. https://doi.org/10.1007/s13277-014-2861-5.

Massagué, J., 2008. TGFβ in Cancer. Cell 134, 215–230. https://doi.org/10.1016/j.cell.2008.07.001.

Murata, T., Ishikawa, Y., Saruul, E., Selenge, E., Sasaki, K., Umehara, K., Yoshizaki, F., Batkhuu, J., 2016. Abietane-type diterpenoids from the roots of *Caryopteris mongolica* and their cholinesterase inhibitory activities. Phytochemistry 130, 152–158. https://doi.org/10.1016/j.phytochem.2016.05.011.

Nieto, M.A., Huang, R.-J., Jackson, R.A., Thiery, J.P., 2016. Emt: 2016. Cell 166, 21–45. https://doi.org/10.1016/j.cell.2016.06.028.

Omori, H., Nishio, M., Masuda, M., Miyachi, Y., Ueda, F., Nakano, T., Sato, K., Mimori, K., Taguchi, K., Hikasa, H., Nishina, H., Tashiro, H., Kiyono, T., Mak, T.W., Nakao, K., Nakagawa, T., Maehama, T., Suzuki, A., 2020. YAP1 is a potent driver of the onset and progression of oral squamous cell carcinoma. Sci. Adv. 6 https://doi.org/10.1126/sciadv.aay3324.

Pastushenko, I., Blanpain, C., 2019. EMT Transition States during Tumor Progression and Metastasis. Trends Cell Biol. 29, 212–226. https://doi.org/10.1016/j.tcb.2018.12.001.

Peng, D., Fu, M., Wang, M., Wei, Y., Wei, X., 2022. Targeting TGF-β signal transduction for fibrosis and cancer therapy. Mol. Cancer 21. https://doi.org/10.1186/s12943-022-01569-x.

Pinheiro Barros, M.C., Sousa Lima, M.A., Braz-Filho, R., Rocha Silveira, E., 2003. 1H and13C NMR assignments of abietane diterpenes from *Aegiphila lhotzkyana*. Magn. Reson. Chem. 41, 731–734. https://doi.org/10.1002/mrc.1236.

Pu, D.B., Wang, T., Zhang, X.J., Gao, J.B., Zhang, R.H., Li, X.N., Wang, Y.M., Li, X.L., Wang, H.Y., Xiao, W.L., 2018. Isolation, identification and bioactivities of abietane diterpenoids from *Premna szemaoensis*. RSC Adv. 8 (12), 6425–6435. https://doi.org/10.1039/c7ra13309j.

Ran, X., Yang, K., 2017. Inhibitors of the PD-1/PD-L1 axis for the treatment of head and neck cancer: current status and future perspectives. Drug Des. Devel. Ther. 11, 2007–2014. https://doi.org/10.2147/dddt.S140687.

Rodríguez, B., 2002. Complete assignments of the ^{1}H and ^{13}C NMR spectra of five rearranged abietane diterpenoids. Magn. Reson. Chem. 40, 752–754. https://doi.org/10.1002/mrc.1070.

Škubník, J., Pavlíčková, V.S., Ruml, T., Rimpelová, S., 2021. Vincristine in combination therapy of cancer: emerging trends in clinics. Biology 10. https://doi.org/10.3390/biology10090849.

Song, D., Wang, L., Su, K., Wu, H., Li, J., 2021. WISP1 aggravates cell metastatic potential by abrogating TGF-β-Smad2/3-dependent epithelial-to-mesenchymal transition in laryngeal squamous cell carcinoma. Exp. Biol. Med. 246, 1244–1252. https://doi.org/10.1177/1535370221992703.

Stockert, J.C., Horobin, R.W., Colombo, L.L., Blázquez-Castro, A., 2018. Tetrazolium salts and formazan products in Cell Biology: Viability assessment, fluorescence imaging, and labeling perspectives. Acta Histochem. 120, 159–167. https://doi.org/10.1016/j.acthis.2018.02.005.

Sun, L., 2009. TGFβ signaling supports survival and metastasis of endometrial cancer cells. Cancer Manag. Res. 1, 15–24. https://doi.org/10.2147/cmar.S4545.

Sun, Z., Su, Z., Zhou, Z., Wang, S., Wang, Z., Tong, X., Li, C., Wang, Y., Chen, X., Lei, Z., Zhang, H.T., 2022. RNA demethylase ALKBH5 inhibits TGF-β-induced EMT by regulating TGF-β/SMAD signaling in non-small cell lung cancer. FASEB J. 36 https://doi.org/10.1096/fj.202200005RR.

Tian, X.-D., Min, Z.-D., Xie, N., Lei, Y., Tian, Z.-Y., Zheng, Q.-T., Xu, R.-N., Tanaka, T., Iinuma, M., Mizuno, M., 1993. Abietane Diterpenes from Clerodendron cyrtophyllum. Chem. Pharm. Bull. 41, 1415–1417. https://doi.org/10.1248/cpb.41.1415.

Topalian, S.L., Taube, J.M., Pardoll, D.M., 2020. Neoadjuvant checkpoint blockade for cancer immunotherapy. Science 367. https://doi.org/10.1126/science.aax0182.

Wang, J., Jiang, C., Li, N., Wang, F., Xu, Y., Shen, Z., Yang, L., Li, Z., He, C., 2020a. The circEPSTI1/mir-942-5p/LTBP2 axis regulates the progression of OSCC in the background of OSF via EMT and the PI3K/Akt/mTOR pathway. Cell Death Dis. 11 https://doi.org/10.1038/s41419-020-02851-w.

Wang, L., Song, Y., Wang, H., Liu, K., Shao, Z., Shang, Z., 2020b. MiR-210-3p-EphrinA3-PI3K/AKT axis regulates the progression of oral cancer. J. Cell Mol. Med. 24, 4011–4022. https://doi.org/10.1111/jcmm.15036.

Wang, W.-X., Xiong, J., Tang, Y., Zhu, J.-J., Li, M., Zhao, Y., Yang, G.-X., Xia, G., Hu, J.-F., 2013. Rearranged abietane diterpenoids from the roots of *Clerodendrum trichotomum* and their cytotoxicities against human tumor cells. Phytochemistry 89, 89–95. https://doi.org/10.1016/j.phytochem.2013.01.008.

Wang, P., Yu, J., Yin, Q., Li, W., Ren, X., Hao, X., 2012. Rosiglitazone suppresses glioma cell growth and cell cycle by blocking the transforming growth factor-beta mediated pathway. Neurochemical Research. 37, 2076–2084. https://doi.org/10.1007/s11064-012-0828-8.

Xiao, T., Bao, J., Tian, J., Lin, R., Zhang, Z., Zhu, Y., He, Y., Gao, D., Sun, R., Zhang, F., Cheng, Y., Shaletanati, J., Zhou, H., Xie, C., Yang, C., 2023. Flavokawain A suppresses the vasculogenic mimicry of HCC by inhibiting CXCL12 mediated EMT. Phytomedicine 112. https://doi.org/10.1016/j.phymed.2023.154687.

Xie, F., Zhou, X., Li, H., Su, P., Liu, S., Li, R., Zou, J., Wei, X., Pan, C., Zhang, Z., Zheng, M., Liu, Z., Meng, X., Ovaa, H., Ten Dijke, P., Zhou, F., Zhang, L., 2022. USP8 promotes cancer progression and extracellular vesicle-mediated CD8+ T cell exhaustion by deubiquitinating the TGF-beta receptor TbetaRII. EMBO J. 41, e108791. https://doi.org/10.15252/embj.2021108791.

Xu, M., Shen, L., Wang, K., Du, Q., 2010. A new abietane diterpenoid from *Clerodendrum kaichianum* Hsu. J. Chem. Res. 34, 722–723. https://doi.org/10.3184/030823410x12857507693455.

Yang, G., Ma, H., Che, M., Zhang, J., 2018. Study on Stability of the antimicrobial activity from leaves of *Clerodendrum mandarinorum* Diels volatile Oil. Guangdong Chemical Industry 45, 83–84.

Zeboudj, L., Sideris-Lampretsas, G., Silva, R., Al-Mudaris, S., Picco, F., Fox, S., Chambers, D., Malcangio, M., 2023. Silencing miR-21-5p in sensory neurons reverses neuropathic allodynia via activation of TGF-β–related pathway in macrophages. J. Clin. Investig. 133 https://doi.org/10.1172/jci164472.

Zhang, L., Song, J., Kong, L., Yuan, T., Li, W., Zhang, W., Hou, B., Lu, Y., Du, G., 2020. The strategies and techniques of drug discovery from natural products. Pharmacol. Ther. 216 https://doi.org/10.1016/j.pharmthera.2020.107686.

Zheng, Y., Wang, Z., Xiong, X., Zhong, Y., Zhang, W., Dong, Y., Li, J., Zhu, Z., Zhang, W., Wu, H., Gu, W., Wu, Y., Wang, X., Song, X., 2018. Membrane-tethered Notch1 exhibits oncogenic property via activation of EGFR–PI3K–AKT pathway in oral squamous cell carcinoma. J. Cell. Physiol. 234, 5940–5952. https://doi.org/10.1002/jcp.27022.

Zhu, M., Bowery, N.G., Greengrass, P.M., Phillipson, J.D., 1996. Application of radioligand receptor binding assays in the search for CNS active principles from Chinese medicinal plants. J. Ethnopharmacol. 54 (2–3), 153–164. https://doi.org/10.1016/s0378-8741(96)01454-7.